Preparation of Hydroxyapatite Scaffolds from Cockle Shell for Bone repair

Sittiporn Punyanitya, M.D.[1], Rungsarit Koonawoot, Ph.D.[2], Anucha Raksanti, Ph.D.[3], Phanlob Chankachang, Ph.D.[4]
[1]Innovative Biomaterials and Medical Device Research Group, Mae Fah Luang University, Chiang Rai, Thailand 57100
[2]Boonyapanit Co., Ltd., 19/44, Singharaj Road, Tumbol Sriphum, Amphur Muang Chiang Mai, Thailand 50200
[3]Multidisciplinary Research Institute, Chiang Mai University, Chiang Mai, Thailand 50200
[4]Faculty of Management Science, Sakon Nakhon Rajabhat University, Sakon Nakhon, Thailand 41000
Received 14 November 2024 • Revised 13 February 2025 • Accepted 16 February 2025 • Published online 1 May 2025

Abstract:

Background: There is a growing demand for effective bone repair materials to replace and reduce the import of materials from abroad, utilizing waste materials from natural resources in Thailand. The goal is to create medical devices and develop inventions into innovations that can be commercialized.

Objectives: This study aimed to prepare hydroxyapatite (HA) scaffolds using a solid-state reaction with raw materials of $CaCO_3$ and $NH_4H_2PO_4$.

Materials and Method: Scaffolds were synthesized under two conditions with sintering temperatures ranging from 1100 to 1300°C for 2 hours. The phase contents, physical, and mechanical properties were investigated. Additionally, to evaluate the maximum HA phase content, each condition was assessed in the subcutaneous soft tissue of laboratory rats over 7, 30, and 90 days. Characterization techniques included XRD, SEM, porosity analysis, bending strength testing, hardness measurement, and histological studies using optical microscopy.

Results: The findings indicated that the scaffolds sintered at 1300°C for 2 hours (Condition 2) had the highest HA content. After 90 days, the scaffold's reaction with soft tissues showed mild inflammation and good tissue compatibility due to the high HA content.

Conclusion: Our results conclude that HA scaffolds prepared from cockle shells have potential for use as bone grafts, as the samples were found to be nontoxic and biocompatible with soft tissues.

Keywords: Bone graft, Cockle shells, Scaffolds, Soft tissue, Histological

Corresponding author: Sittiporn Punyanitya, M.D.
School of Medicine, Mae Fah Luang University, Chiang Rai, Thailand 57100
E-mail: punyanitya.s@gmail.com
GMSMJ 2025; 5 (2): 85-99

Introduction

Calcium phosphate bioinorganics are compounds that are widely studied for orthopedic applications. The most widely used of these compounds include hydroxyapatite (HA), β-tricalcium phosphate (β-TCP), and biphasic calcium phosphate (BCP).[1] HA is one of the most effective biocompatible materials and is found to be the major component of bone. A quantitative XRD analysis should indicate a minimum HA content of 95% in relative peak intensities for surgical implants.[2] HA has been widely used as a bone graft for bone replacement, substitution, or proliferation. The need for bone grafts depends on the complexity of the bone defects. For instance, if the defect is minor, bone has its own potential to self-remodel within a few weeks. Therefore, surgery is not required. However, in the case of severe defects and loss of bone volume, the bone cannot heal on its own. In such cases, grafting is necessary to restore function without damaging living tissues.[3,4] The preliminary study in this work focused only on the soft tissue reaction to HA scaffolds, evaluating their biocompatibility and safety for soft tissues. The hard tissue reaction to the implanted sample has not yet been studied, as this will be the focus of future research. Furthermore, studying the reaction of the sample to soft tissue is crucial when developing bone grafts, as the HA scaffold not only interacts with bone but also with the surrounding soft tissue. Therefore, the results of this study may be applied in the future for human bone grafts. Scaffolds are made from HA powders, which are synthesized using several methods such as the wet method[5], sol-gel[6], hydrothermal[7], aqueous precipitation[8], and solid-state reaction.[9-11] Solid-state reaction is a decomposition reaction of two reactants: a solid mixture of $CaCO_3$ and phosphate, and it provides appropriate mechanical and thermal energy to the mixture to synthesize HA ceramics. However, there is limited research on the solid-state reaction method because the reaction tends to produce adhesion forces between fine particles, which readily agglomerate. Nevertheless, this method is very simple, low-cost, and highly productive. The advantages of using calcium carbonate ($CaCO_3$) from cockle shells, instead of synthetic sources, include a very low raw material cost. In addition, the product yield from this method is very high. Therefore, HA produced from cockle shells via the solid-state reaction method can be a viable alternative.

Cockle shells *(Tegillarca granosa)* are natural materials from biological sources, consisting of micro-laminated composites of minerals (95-99% $CaCO_3$) and 1-5% organic macromolecules, which are primarily located within the inter-crystalline boundaries. In addition, the unique composition and composite microstructure of cockle shells result in an enhancement in toughness by three orders of magnitude compared to non-biogenic $CaCO_3$.[12] Therefore, the aim of this work is to study HA scaffolds derived from cockle shells, investigate their properties, and examine the reaction of optimized samples to subcutaneous soft tissue.

Materials and Methods

Materials

Cockle shells were purchased from a commercial seafood market in Chiang Rai, Thailand. Hydrogen peroxide (H_2O_2) (50%), stearic acid, and ethanol (95%) were purchased from World Chemical Group Co. Ltd., Thailand. Tiletamine, zolazepam, xylazine HCl, povidone iodine, penicillin G, and streptomycin were obtained from Sigma-Aldrich, Thailand. Analytical-grade $NH_4H_2PO_4$ was purchased from Merck, Germany.

Samples preparation

Cockle shells were treated with H_2O_2 solution, rinsed with distilled water, oven-dried at 80°C for 24 hours, and finally calcined in air at 550°C for 5 hours. The $CaCO_3$ powder derived from cockle shells was ground and screened through a 325 mesh.[13] The starting powders were combined in precise quantities: 0.58 mole of $CaCO_3$ powder and 0.36 mole of $NH_4H_2PO_4$ powder for Condition 1, and 0.59 mole of $CaCO_3$ powder and 0.35 mole of $NH_4H_2PO_4$ powder for Condition 2. The composition of the preparation is shown in Table 1.

Table 1 The composition for preparation of HA

Condition	Reactant compositions	
	$CaCO_3$ (Mole)	$NH_4H_2PO_4$ (Mole)
1	0.58	0.36
2	0.59	0.35

In the first step, $CaCO_3$ powder was mixed with $NH_4H_2PO_4$ powder in a nylon polyamide milling jar with yttrium-stabilized zirconia grinding media. The jar was then placed in a planetary ball mill for 45 minutes. In the second step, the obtained powder was pressed using an uniaxial pressing machine into a disc shape with dimensions of 4 mm in thickness and 16.5 mm in diameter, under a stress of approximately 3 MPa in a cylindrical stainless steel die. The die wall was lubricated with a liquid solution of 5 wt% stearic acid in ethanol. Finally, the green bodies of the samples were sintered at temperatures of 1100, 1150, 1200, 1250, and 1300°C for 2 hours in an electric furnace (Eurotherm controller 3504, U.S.A.). Sintering was carried out with a heating ramp rate of 60°C/h up to 400°C, followed by a soaking time of 30 minutes. The temperature was then increased at a ramp rate of 120°C/h up to 650°C, with a soaking time of 1 hour. Next, the heating rate was increased to 300°C/h, and the sample was isothermally sintered at different temperatures with soaking times ranging from 2 to 5 hours. Afterward, the temperature was decreased with a ramp rate of 120°C/h to 850°C, where it was held for 1 hour. Finally, the furnace was turned off, allowing the samples to cool to room temperature with a ramp rate of 240°C/h. The scaffold sample is shown in figure 1.

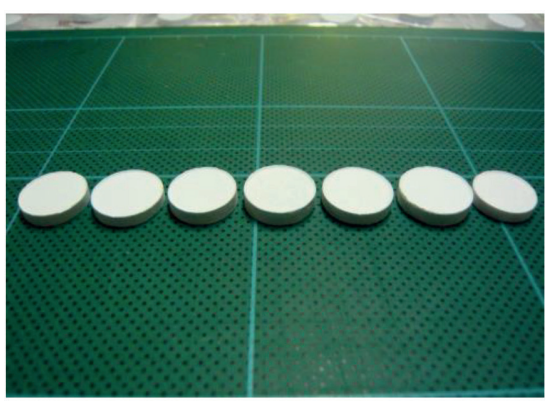

Figure 1 The photographs of scaffolds

Animals testing

This study was approved by the Ethical Committee of the Faculty of Medicine, Chiang Mai University. We adhered to the principles of the 3Rs concerning the use of laboratory animals. Twelve healthy adult Wistar rats (1 to 2 months of age, non-specific gender), weighing approximately 300 to 400 g, were used in this study. These rats were obtained from the Laboratory Animal House, Faculty of Medicine, Chiang Mai University, and we followed the guidelines for the care and use of laboratory animals.[14] Surgery was performed under anesthesia using a mixture of Tiletamine (50 mg/1 c.c.) and Zolazepam (50 mg/1 c.c.) at a dose of 40 mg/kg, along with Xylazine HCl at 5 mg/kg. The dorsal neck area (approximately 1x1 square inch) was shaved, washed, and disinfected with 70% alcohol and povidone iodine solution. The wound was then carefully closed with an absorbable suture to prevent movement of the samples. After surgery, the laboratory rats were allowed to recover from anesthesia. Simultaneously, penicillin G and streptomycin were administered to prevent bacterial contamination, with antibiotic doses of 20,000 IU/kg post-operation. Finally, the individually marked rats were housed in standard cages ($266 \times 425 \times 185$ mm^3 in size, with an area of 820 cm^2).[15]

For the rat trials, the disc scaffolds were cut and lathed into a cylindrical shape, with diameters ranging from 1 to 6 mm and lengths ranging from 10 to 20 mm. The samples used in the animal trials were those prepared under the optimized conditions of Condition 1 and Condition 2. In each rat, two samples were implanted: one under Condition 1 (right side, Group 1) and one under Condition 2 (left side, Group 2). At least four rats, each with two implanted samples, were required for each implantation period. The implantation periods were 7, 30, and 90 days.[16,17] The surgical procedure was as follows: The sample from Condition 1 was implanted on the right side (Group 1) and the sample from Condition 2 was implanted on the left side (Group 2) of the subcutaneous tunnel on the back of the rat's neck. A small incision, approximately 1 cm long, was made on each side of the rat's neck to facilitate implantation.

Characterization

1. The multiple phases of all scaffolds were analyzed using X-ray diffraction (XRD) (Bruker, D8 Advance, England), operated at 40 kV and 30 mA, with Cu Kα radiation (λ = 1.54056 Å). The scanning speed was set to 0.04°/min, and the 2θ range was from 10° to 80°.

2. The microstructure of the HA scaffolds was examined using scanning electron microscopy (SEM) (JEOL, JSM-6335F, Japan). The fracture morphology of the scaffolds was studied using a field emission SEM. The sintered samples were coated with a thin layer of gold (Au) for imaging purposes.

3. The density and porosity of the scaffolds (six samples) were measured using the Archimedes method, with distilled water as the fluid medium.[18] The average grain size was determined using the linear intercept method.[19]

4. Bending strength was investigated using a ball-on-ring test[20] with a universal testing machine (Shimadzu, AGS-500A, Japan). The span length was 20 mm, the crosshead speed was 5 mm/min, and the load cell capacity was 2500 N. Six samples were tested for each condition, and the average result for each condition was calculated. The bending strength (σ) of the samples was determined using Equation (1).

$$\sigma = \frac{3F(1+\nu)}{4\pi t^2}\left[\frac{(1-\nu)}{(1+\nu)} \times \frac{2a^2 - b^2}{2R^2} + 2\ln\left(\frac{a}{b}\right) + 1\right] \quad (1)$$

where σ is the strength in MPa; F is the breaking load in Newtons; ν is Poisson's ratio; a is the radius of the support; R is the radius of the sample; t is the thickness of the sample; and b is t/3.

5. Microhardness measurements were conducted using a Vickers hardness (HV) tester with a pyramidal diamond indenter, applying a 50 g load for 15 seconds. The lengths of the diagonals of the hardness indents were measured using an optical microscope. Five indentations were made for each sample, and the average value was calculated using Equation (2).[21]

$$HV = 0.1891 \frac{F}{d^2} \quad (2)$$

where F is the indentation load in Newtons (N) and d is the mean diagonal length of the indentation in micrometers.

6. Histological analysis was performed following euthanasia. During necropsy, any gross abnormalities in color or consistency were recorded in the tissue surrounding the samples. Each sample, along with the surrounding tissue (at least 4 mm in thickness), was removed. The tissue was then collected in a 10% formalin solution for fixation. Histological examination involved the description of inflammatory cells and the evaluation of the soft tissue response. The results from each histological test were evaluated using optical microscopy.

Statistical analysis

All quantitative data were analyzed with origin 8.0 (OriginLab Corporation, USA) and presented as the mean ± standard deviation. Statistical comparisons were carried out using analysis of variance (ANOVA, Origin 8.0). A value of $p < 0.05$ was considered to be statistically significant.

Results and Discussion

The XRD patterns of the scaffolds obtained from conditions 1 and 2 were recorded after sintering at temperatures ranging from 1100 to 1300°C for 2 hours. The sintered scaffolds were composite ceramics consisting of mixtures of HA, β-TCP, and CaO phases. All patterns were compared with the standard pattern from the JCPDS file no. 09-0432.[22] (Figures 2)

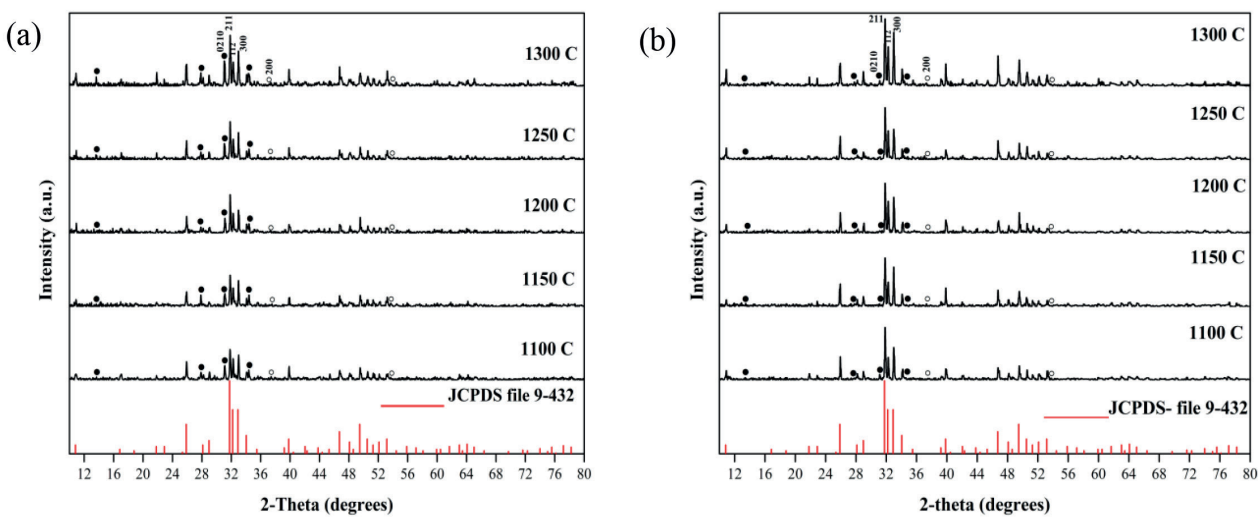

Figure 2 The XRD patterns of the sample powders from condition 1 (a) and condition 2 (b) at various temperatures with the JCPDS file no. 09-0432 of pure HA. The symbols represent β-TCP (•) and CaO (o).

The XRD patterns of the sample powders from condition 1, sintered at various temperatures, were compared with the JCPDS file no. 09-0432 for pure HA. The four dominant HA peaks were observed at $2\theta = 25.9°$ (002), $2\theta = 31.8°$ (211), $2\theta = 32.2°$ (112), and $2\theta = 32.9°$ (300). The peak for the (0210) plane of β-TCP was observed at $2\theta = 31°$ (JCPDS file no. 09-169), while the (200) plane of CaO appeared at $2\theta = 37.35°$ (JCPDS file no. 37-1497). The XRD analysis of the scaffolds obtained from condition 1 is presented in Figure 2(a). The XRD results revealed that the scaffolds contained multiple phases. The crystalline phase content of HA, β-TCP, and CaO in the scaffolds was determined using the reference intensity ratio (RIR) method.[23-25] For the scaffolds from condition 1, the percentage of crystalline phases was found to be: HA (67-69%), β-TCP (25-27%), and CaO (5-7%). The scaffolds from condition 2, presented in Figure 2(b), had the following phase percentages: HA (85-91%), β-TCP (4-8%), and CaO (3-6%). These results suggest that the scaffolds obtained from condition 2 are more likely to form a single-phase HA than those from condition 1 when sintered under the same temperature and time conditions. At various sintering temperatures, the amount of HA increased with the sintering temperature. When sintered at 1300°C for 2 hours, condition 1 reached a maximum of 69% HA, while condition 2 reached 91% HA. The highest HA content (91%) obtained from condition 2 was close to the standard of pure HA (≥ 95%). The effect of composition and sintering temperature on the formation of the HA phase can be explained by the reactions between the starting materials, which resulted in good densification of the mixed powders according to the firing schedule. The microstructure of the scaffolds sintered at different temperatures showed significant variations in crystalline phases. This variation could be influenced by factors such as particle size, isothermal temperature, heating rate, and densification, which serve as driving forces for the synthesis of the HA phase.[26] This is consistent with previous studies, which demonstrated that the formation of β-TCP is faster than that of HA. This is due to the continuous reaction of CaO with the phosphate group to form β-TCP. However, the reaction was carefully controlled in this study by adjusting the time and temperatures in the firing schedule.[27] Additionally, previous studies have reported that the thermal decomposition of synthetic HA, processed between 1160 and 1300°C, leads to its dehydration in two phases. This results in the formation of oxyhydroxyapatite ($Ca_{10}(PO_4)(OH)_{2-2x}O_xV_x$) and oxyapatite ($Ca_{10}(PO_4)6O_x$), where V represents a lattice vacancy in the OH position. Oxyapatite may decompose into a mixture of β-TCP and CaO. In this study, the rehydroxylation of oxyapatite was reversed to HA by the cooling and annealing steps in the firing schedule, although the reversed phase may not have undergone a complete reaction, as HA, β-TCP, and CaO phases were still observed in the XRD analysis.[28]

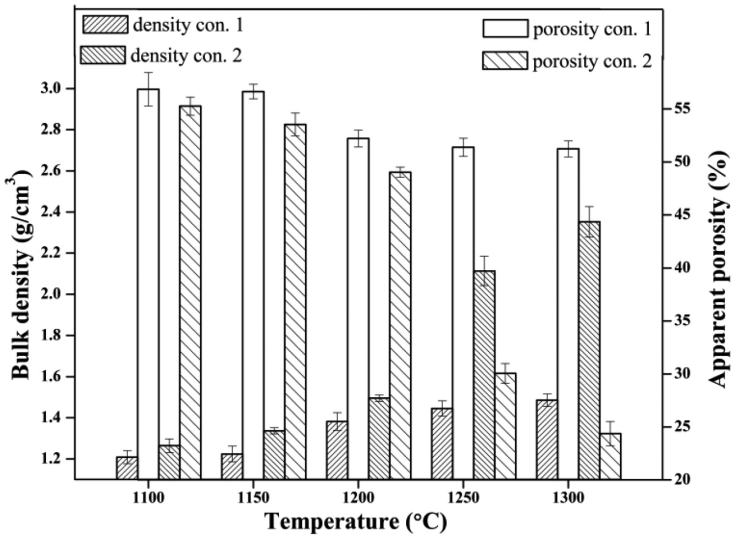

Figure 3 Bulk density and apparent porosity with con. 1 and 2 at different temperatures

Figure 3 displays the physical properties of scaffolds obtained from condition 1 (con.1) and condition 2 (con.2) as a function of temperature. It was found that, for scaffolds from con. 1, as the sintering temperature increased, the bulk density increased, while the apparent porosity decreased. A similar trend was observed for scaffolds from con. 2. The composition and temperature have an effect on the synthesis of HA because the heat causes the calcium and phosphorus particles to bond. As a result, the sample under condition 2 tends to synthesize into HA. The bulk density of con. 2 was 2.375 ± 0.074 g/cm^3, which is lower than the standard value for pure HA (3.16 g/cm^3). However, this value is higher than the density of natural cortical bone (1.8-2.0 g/cm^3) and natural cancellous bone (0.1-1.0 g/cm^3). This can be explained by the fact that the bulk density of the scaffold includes the volume of the solid phase, as well as both open and closed pores, while the density of pure HA represents only the solid phase. Nevertheless, the bulk density of the scaffold falls within the density range of natural bone (both cortical and cancellous bone), which also consists of solid mass with open and closed pores. Both conditions yielded porous materials with open and closed pores. It was observed that the densification of scaffolds from con. 1 resulted in slight shrinkage of the bodies when sintered at 1100-1300 °C, which corresponded to minimal changes in bulk density and apparent porosity. In contrast, scaffolds from con. 2 exhibited slight shrinkage at 1100-1200°C, but showed more significant shrinkage at 1250°C and 1300°C.

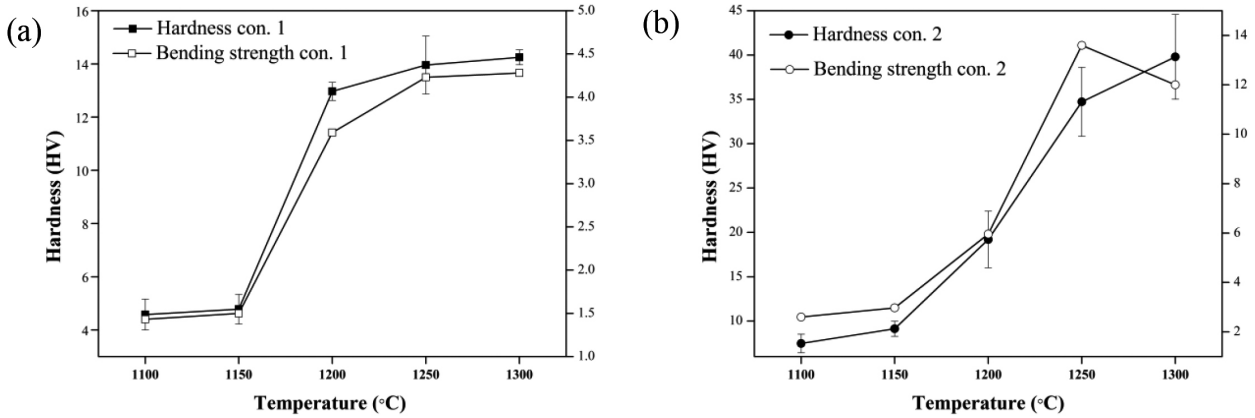

Figure 4 Vickers hardness and bending strength with con. 1 (a) and con. 2 (b) as a function of temperature

Figure 4 (a) shows the variation in the Vickers hardness and bending strength of the samples from con. 1 was a function of temperature. An increase in both characteristics was observed with rising temperatures. The Vickers hardness increased from 4.58 ± 1.15 HV at 1100°C to 14.25 ± 0.55 HV at 1300°C for con. 1. The bending strength of the scaffolds increased from 1.43 ± 0.39 MPa at 1100°C to 4.28 ± 0.40 MPa at 1300°C. Figure 4(b) shows the evolution of the Vickers hardness and bending strength of the samples from con. 2 was a function of temperature which similar to con. 1, and increase in both characteristics was observed with increasing temperature. The Vickers hardness increased from 7.48 ± 2.10 HV at 1100°C to 39.80 ± 9.56 HV at 1300 °C for con. 2. Meanwhile, the bending strength of the scaffolds increased from 2.60 ± 0.59 MPa at 1100°C to 13.60 ± 1.55 MPa at 1250°C, before decreasing slightly to 12.00 ± 1.21 MPa at 1300°C. This decrease in bending strength at 1300°C may be attributed to the reduction in closed pores and the increase in finer grain sizes at higher temperatures. Additionally, the formation of pores after the dehydroxylation of HA, leading to the formation of oxyapatite, could also contribute to this phenomenon. The maximum average Vickers hardness was 39.80 ± 9.56 HV at 1300°C for con. 2, which is lower than the theoretical value of 600 HV for pure HA. However, this value is close to the hardness of natural cortical bone (40.4 HV) and higher than that of natural cancellous bone (35.2 HV). The bending strength was 13.60 ± 1.55 MPa at 1250°C for con. 2, which is lower than the theoretical range of 115-200 MPa for pure HA.

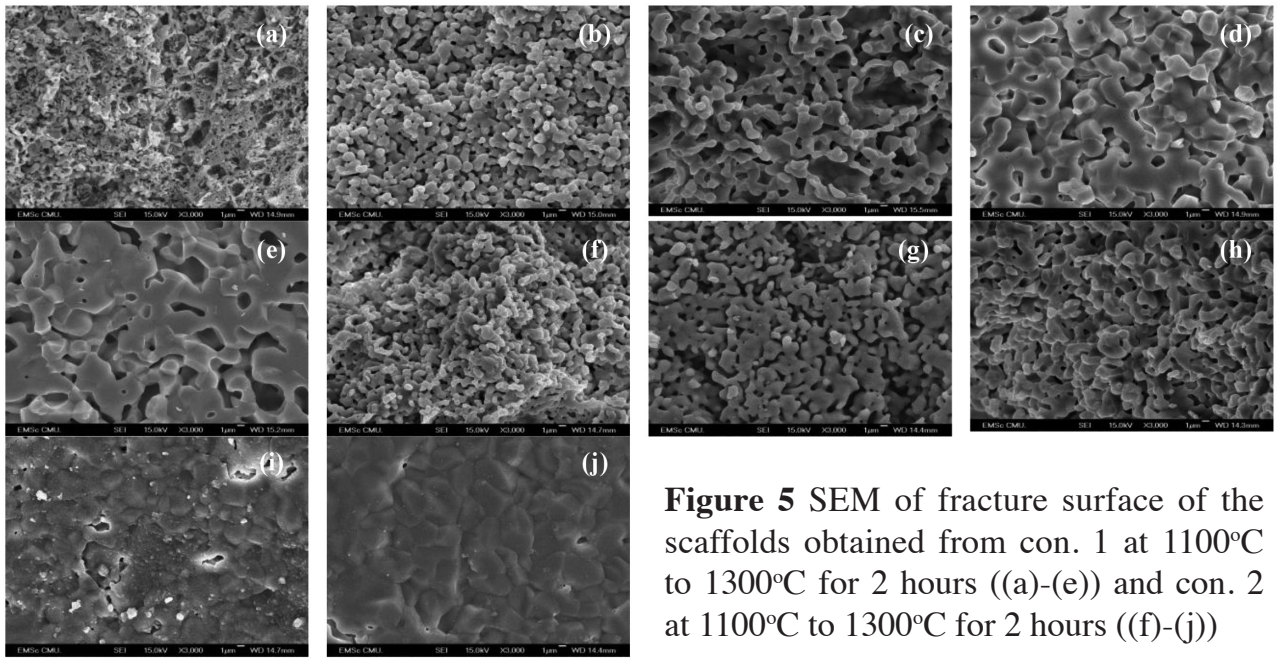

Figure 5 SEM of fracture surface of the scaffolds obtained from con. 1 at 1100°C to 1300°C for 2 hours ((a)-(e)) and con. 2 at 1100°C to 1300°C for 2 hours ((f)-(j))

The SEM images of the scaffolds obtained from con. 1 and con. 2 are illustrated in Figure 5. The micrographs show that the average grain size of the scaffold obtained with con. 1 was 0.3 μm, and the average pore size ranged from 0.4 - 6 μm. The porosity and pore size of the obtained scaffold were measured by image analysis and the Archimedes principle. The porosity of the sample was approximately 57% at 1100°C (Figure 5(a)). For the scaffold obtained from con. 2, the average grain size was 0.6 μm, the average pore size ranged from 1 to 10 μm, and the porosity was approximately 53% (Figure 5(f)). The fracture surfaces of the scaffolds obtained from con. 1, sintered at 1150°C, showed an increase in grain size, with an average range of 0.3 - 0.8 μm. The average pore size was 6 μm, and the porosity was approximately 56% (Figure 5(b)). For the scaffolds obtained from con. 2, the average grain size was 0.9 μm, the average pore size was 7 μm, and the porosity was approximately 51% (Figure 5(g)). At 1200°C, the fracture surface of the scaffolds obtained from con. 1 showed an increase in grain size, ranging from 0.8 to 13 μm. The average pore size was 7.2 μm, and the porosity was approximately 52% (Figure 5(c)). For con. 2, the average grain size was 1.5 μm, the average pore size was 2.2 μm, and the porosity was approximately 50% (Figure 5(h)). This temperature led to the formation of smaller pores, ranging in size from 1 to 2 μm, alongside the development of larger pores ranging from 3 to 8 μm. In addition, the formation of closed pores began at this temperature. At 1250°C, the fracture surface of the scaffolds obtained from con. 1 showed an average grain size of 3.5 μm, an average pore size of 4.2 μm, and a porosity of approximately 51% (Figure 5(d)). For the scaffolds obtained from con. 2, the average grain size was 2.7 μm, the average pore size was 1.5 μm, and the porosity was approximately 33% (Figure 5(i)). At 1300°C, the fracture surface of the scaffolds from con. 1 showed an average grain size of 5.9 μm, an average pore size of 5.2 μm, and a porosity of approximately 50% (Figure 5(e)). For con. 2, the average grain size was 7.9 μm, the average pore size was 0.5 μm, and the porosity was approximately 26% (Figure 5(j)). Grain growth was clearly observed at this temperature.

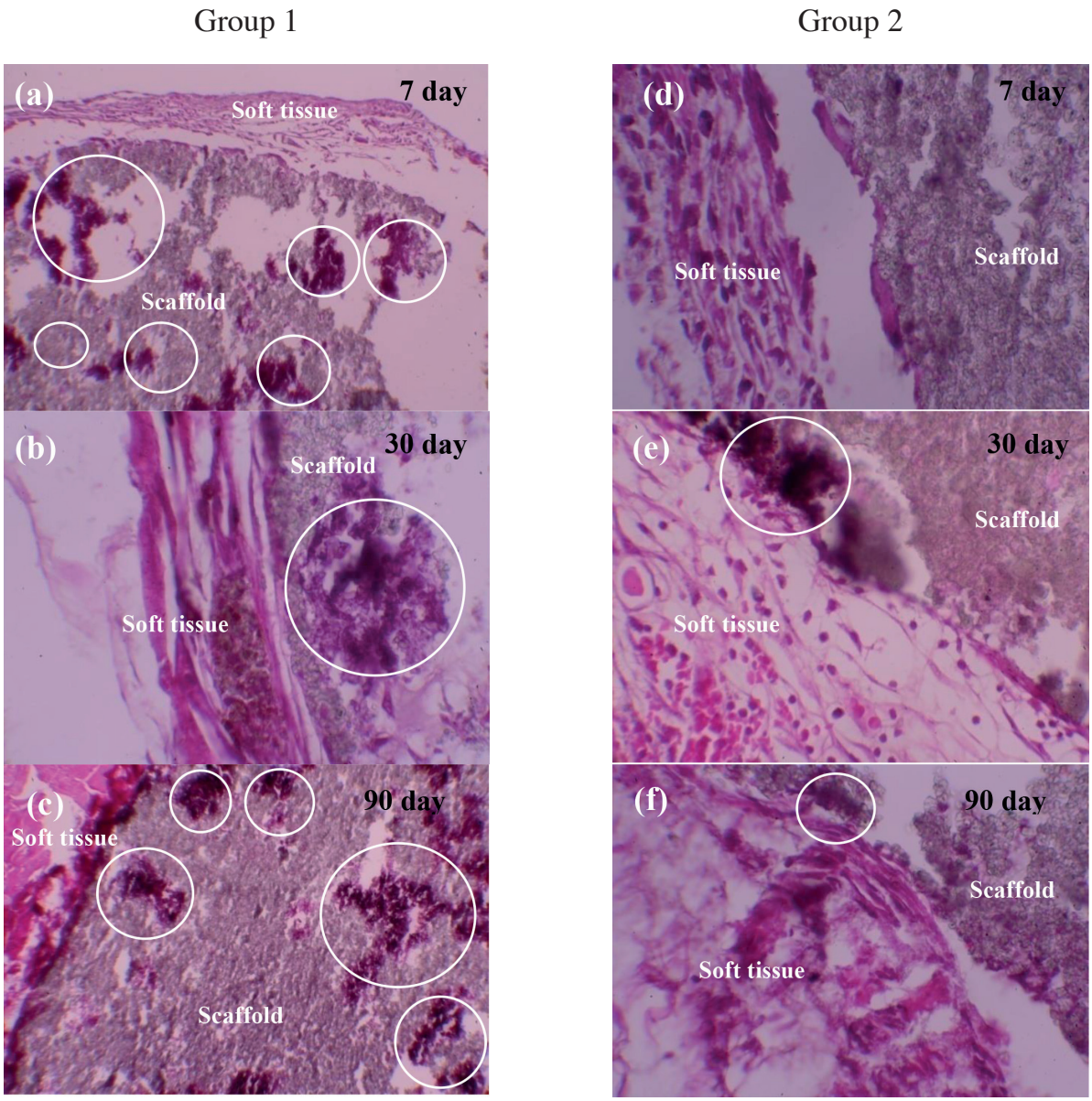

Figure 6 Optical microscope images of scaffolds obtained from Group 1 ((a)-(c)) and Group 2 ((d)-(f)) with magnification of X40

The results of animal testing show the tissue response to the scaffolds after implantation for 7, 30, and 90 days (Figure 6). Microscopic examination of the sections revealed fragments of the scaffolds from Group 1 and Group 2, surrounded by fibro-adipose tissue.

At 7 days after implantation, Group 1 showed a mild foreign body reaction with mixed cellular inflammatory infiltration and the presence of fibroblasts. In contrast, Group 2 exhibited a moderate foreign body reaction, with minimal epithelioid cells and occasional small monocytoid foreign body giant cells. Additionally, cellular infiltration into the scaffold bodies was observed in Group 1, but was absent in Group 2 (Figure 6 (a) and (d)). This difference can be attributed to the lower porosity of the scaffolds in Group 2, as high porosity promotes cellular infiltration into the scaffold bodies. This phenomenon highlights the potential of Group 1 scaffolds as a suitable material for bone grafting, as

previously discussed in.[29] Furthermore, dystrophic calcification was observed in the bulk scaffolds of Group 1, but was absent in Group 2. This difference is due to the higher amount of the CaO phase (circled) in Group 1, as confirmed by XRD analysis. The circled areas contained calcium salts that were deposited among the injured tissues and other phases of the scaffold. These calcium salts were visible to the naked eye as purple, non-cellular lesions on routine histology. In addition, the degradation of scaffold components into the surrounding host tissues was observed in both groups through XRD analysis. However, Group 2 exhibited lower amounts of β-TCP phases compared to Group 1 at 1300°C for 2 hours. This phenomenon has been previously explained in.[30,31]

At 30 days post-implantation, the inflammatory response to the scaffolds in Group 1 was moderate, while in Group 2, it was mild. Group 2 showed a decrease in inflammatory cells, while Group 1 exhibited an increase in inflammatory cells within the scaffold bodies. Additionally, cellular infiltration was present in the bodies of Group 1 but absent in Group 2, which had lower porosity compared to Group 1. Furthermore, dystrophic calcification was observed in both Group 1 and Group 2, as the CaO phase (circled) remained present in both scaffold bodies. Finally, the degradation of scaffold components into the surrounding host tissues was evident in both groups, likely due to the high solubility of β-TCP in the scaffold bodies (Figure 6(b) and (e)).

At 90 days post-implantation, the inflammatory response to the scaffolds in Group 1 was severe, with the appearance of some epithelioid cells and large multinucleated foreign body giant cells. In contrast, Group 2 exhibited a mild inflammatory response. Group 2 showed a consistent level of inflammatory cells, while Group 1 exhibited an increase in inflammatory cells within the scaffold bodies (Figure 6(c) and (f)). This difference may be attributed to the higher amount of β-TCP phase in the structure of Group 1, which likely contributed to the higher solubility of the scaffolds. Additionally, cellular infiltration was present in Group 1 but absent in Group 2, likely due to the significant difference in porosity between the two groups. Dystrophic calcification was observed in the bulk of both Group 1 and Group 2 scaffolds, as the CaO phase (circled) remained present in both. However, small areas of calcification were found in the microstructure of Group 2, while large areas of calcification were observed in Group 1. Moreover, the degradation of scaffold components into the surrounding host tissues was observed in Group 1 but absent in Group 2. This difference may be due to Group 2 starting to stabilize in the soft tissues of the rats, whereas Group 1 remained unstable due to the continuous dissolution of ceramic components.

Table 2 Phenomenon of foreign body reaction and some changes of tissues

Tissue reaction	Time periods (days)			
	Group	7	30	90
Reaction grading	1	♦	♦♦	♦♦♦
	2	♦♦	♦	♦
Cellular infiltration into ceramic body	1	√	√	√
	2	⊗	⊗	⊗
Calcification in ceramic body	1	√	√	√
	2	⊗	√	√
Displacement of ceramic components into surrounding host tissue	1	√	√	√
	2	√	√	⊗

Note: Foreign body reaction grading; Symbol (♦) is mild reaction, (♦♦) is moderate reaction and (♦♦♦) is severe reaction.
Cellular infiltration, calcification and displacement of ceramic components; Symbol (√) is absent and (√) is present.

Table 2 presents the overall changes observed over the time period from 7 to 90 days. The scaffolds obtained from Group 2 exhibited lower levels of inflammation compared to those from Group 1. This result supports the finding that Group 2 had a higher HA content than Group 1, which could explain the greater stability of the scaffolds in Group 2. In contrast, Group 1 demonstrated resorbable behavior due to the higher amount of β-TCP phase compared to Group 2. These findings are consistent with previous studies, which reported that the solubility rate of pure HA sintered in subcutaneous tissue was 0.1 mg/year, whereas β-TCP is a resorbable material that dissolves much faster than pure HA 12.3 times faster in an acidic solution and 22.3 times faster in a basic medium.[30,31] The apparent porosity of Group 1 was 51.2%, indicating that it is a porous material, while Group 2 had an apparent porosity of 24.37%, making it a relatively dense material. Apparent porosity is a crucial parameter that supports cellular infiltration into the scaffold bodies. SEM analysis of Group 2 revealed pore sizes ranging from 1 to 10 μm, but no cellular infiltration was observed. According to[29], scaffolds made of HA with 52% porosity implanted in the bone of laboratory rats allowed bone cells to rapidly grow into the scaffold. Calcification was another factor that inhibited cellular infiltration into the scaffold bodies of Group 2, as the CaO phase remained present in the microstructure. However, we hypothesize that cells from surrounding tissues may have occupied the scaffold bodies, because after implantation, the high solubility of β-TCP in the body fluid of the rats likely caused the smaller pores to enlarge over time.

Conclusion

Cockle shells were converted into calcium phosphate scaffolds with various HA and β-TCP compositions via solid-state reaction. The aim of the research is to synthesize HA through a solid-state process, which requires HA to be more than 95%. However, the synthesis results from this process revealed the formation of secondary phases, namely TCP and CaO. The phase composition of the HA scaffolds depended

on the concentration of $CaCO_3$ and phosphorus precursors, as well as the sintering temperature. The optimized conditions were those that resulted in the highest quantity of HA, which in turn influenced the physical, mechanical, and biological properties of the scaffolds. A comparison of the phase content, physical, and mechanical properties of scaffolds obtained from conditions 1 and 2 revealed that the highest HA content was 69% for condition 1 and 91% for condition 2, both sintered at 1300°C for 2 hours. The impurities in the scaffolds from condition 1 included 25.10% β-TCP and 5.76% CaO, while in condition 2, the impurities were reduced to 5.18% β-TCP and 3.38% CaO. Furthermore, condition 2 demonstrated greater potential for synthesis and exhibited superior physical and mechanical properties, making it more suitable for human bone repair compared to condition 1. The scaffold obtained from Group 1 and Group 2 was non-toxic and biocompatible with soft tissues. Group 2 scaffolds exhibited fewer inflammatory cells than those from Group 1, were more stable, and showed greater potential for use as bone grafts. However, the scaffolds from Group 2 had smaller pore sizes (lower than the theoretical range of 100-500 μm) and a lower percentage of porosity compared to the ideal parameters for bone tissue engineering.

Acknowledgements

This work was supported by the Innovative Biomaterials and Medical Device Research Group, Mae Fah Luang University. The authors would like to thank Boonyapanit Co., Ltd., the Multidisciplinary Research Institute at Chiang Mai University, and the Faculty of Management Science, Sakon Nakhon Rajabhat University, for their support in this study.

References

1. Palmer LC, Newcomb CJ, Kaltz SR, Spoerke ED, and Stupp SI, Biomimetic Systems for Hydroxyapatite Mineralization Inspired by Bone and Enamel. Chem Rev. 2008; 108 (11): 4754-83.
2. ASTMF1185-03. Standard Specification for Composition of Hydroxyapatite for Surgical Implants, West Conshohocken, PA, USA. 2009, pp. 475-477.
3. Murugan R and Ramakrishna S. Development of nanocomposites for bone grafting. Comp Sci Tech. 2005: 65 (15-16): 2385-406.
4. Vecchio KS, Zhang X, Massie JB, Wang M, and Kim CW. Conversion of bulk seashells to biocompatible hydroxyapatite for bone implants. Acta Biomater. 2007; 3 (6): 910-8.
5. Raynaud S, Champion E, Bernahe-Assollant D, and Thomas P. Calcium phosphate apatite with variable Ca/P atomic ratio I. Synthesis, characterization and thermal stability of powders. Biomater. 2002; 23 (4): 1065-72.
6. Balamurugan A, Kannan S, and Rajeswari S. Bioactive sol-gel hydroxyapatite surface for biomedical application-in vitro study. Trends in Biomaterials and Artificial Organs. 2002; 16 (1): 18-20.
7. Zhang X, and Vecchio KS. Creation of dense hydroxyapatite (synthetic bone) by hydrothermal conversion of seashells. Materials Science and Engineering: C. 2006; 26: 1445-50.
8. Rodriquez-Lorenzo LM, Vallet-Regi M, and Ferreira JMF. Fabrication of hydroxyapatite bodies by uniaxial pressing from a precipitated powder. Biomaterials. 2001; 22 (6): 583-8.

9. Rao RR, Roopa HN and Kannan TS. Solid state synthesis and thermal stability of HAP and HAP-β-TCP composite ceramic powders. J Mater Sci: Materials in Medicine. 1997; 8 (8): 511-8.
10. Cox SC, Mallick KK and Walton RI. Comparison of techniques for the synthesis of hydroxyapatite, Bioinspired, Biomimetic and Nanobiomaterials. 2014; 4 (1): 37-47.
11. Pramanik S, Agarwal AK, Rai KN, Garg A. Development of high strength hydroxyapatite by solid-state-sintering process. Ceramic International. 2007; 33, (3): 419-26.
12. Kaplan DL. Mollusc shell structures: Novel design strategies for synthetic materials. Current Opinion in Solid State and Materials Science. 1998; 3: 232-6.
13. Koonawoot R, Thiansem S, and Punyanitya S. Preparation and Characterization of Hydroxyapatite Powder from Mollusc Shells. Pure and Applied Chemistry International Conference (PACCON 2012), pp. 190-193.
14. Committee for the Update of the Guide for the Care and Use of Laboratory Animals, "Guide for the Care and Use of Laboratory Animals, 8th Ed. The National Academy of Sciences, Washington, DC, 2011.
15. Department of Health Education and Welfare, The Guide for Care and Use of Laboratory Animals, Publication (No.78-23). Available from Superintendent of Documents, U.S. Government Printing Office, Washington, 20402. 1978.
16. ASTM F981-04. Standard Practice for Assessment of Compatibility of Biomaterials for Surgical Implants with Respect to Effect of Materials on Muscle and Bone. 2010.
17. ASTM F763-04, Standard Practice for Short-Term Screening of Implant Materials. 2010.
18. Callut S, and Knowles JC. Correlation between structure and compression strength in reticulated glass-reinforced hydroxyapatite foam, Journal of Material Science: Material in Medicine. 2000; 13 (5): 485-9.
19. ASTM E 112-10. Standard Test Method for Determining Average Grain Size. 2010.
20. De With G, and Wagemans HHM. Ball-on-ring test revisited. Journal of the American Ceramic Society. 1989; 72 (8): 1538-41.
21. Callister WD. Fundamentals of Material Science and Engineering. Willey, New York.2001.
22. JCPDS-ICDD Card no.9-432. International center for diffraction data, Newton Square, PA. 2000.
23. Raynaud S, Champion E, Bernache-Assollant D and Laval JP. Determination of Calcium/Phosphorus Atomic Ratio of Calcium Phosphate Apatites Using X-ray Diffractometry. Journal of the American Ceramic Society. 2001; 84 (2): 359-66.
24. How YM, Kasim SR, Akil HM and Ahmad ZA. Effect of $CaCO_3$ Particle Size in Synthesis of β-TCP Powder. Journal of Nuclear and related Technologies. 2009; 6 (1): 19-24.
25. Farzadi A, Solati-Hashjin M, Bakhshi F and Aminian A. Synthesis and characterization of hydroxyapatite/β-tricalcium phosphate nanocomposite using microwave irradiation. Ceramics International. 2011; 37 (1): 65-71.
26. Rahaman MN. Ceramic Processing And Sintering, 2nd Ed., Marcel Dekker, New York. 2003, pp. 754-755.
27. Yang X and Wang Z. Synthesis of biphasic ceramics of hydroxyapatite and β-tricalcium phosphate with controlled

phase content and porosity. Journal of Materials Chemistry. 1998; 8 (10): 2233-7.
28. Guo D, Xu K and Han Y. Influence of cooling modes on purity of solid-state synthesized tetracalcium phosphate. Materials Science and Engineering: B. 2005; 116 (2): 2, 175-81.
29. De Bruijn JD, Sleijster M, Doel MVD, Apeldoorn AV, d Brink IV, Blitterswijk CV, et al. Porous hydroxyapatite scaffold coated with in vitro formed bone-like matrix induct faster bone formation as compared to cell seeded scaffold. Poster of the 47th annual meeting, Feb. 25-28, Ortho. Res. Soc., San Francisco, California. 2001.
30. Wang M. Bioactive materials and processing. Berlin, Heidelberg, Springer Verlag. 2004: pp. 1-82.
31. Jarcho M. Calcium phosphate ceramics as hard tissue prosthetics. Clinical Orthopaedics and Related Research. 1981; 157: 259-78.